Reactions to resolved states and to non-fusion channels for $^{16}O+^{48}Ca$ at $E_{lab}=158.2$ MeV

T. J. Humanic, H. Ernst, W. Henning, and B. Zeidman
Argonne National Laboratory, Argonne, Illinois 60439
(Received 22 March 1982)

In a study of the system $^{16}O+^{48}Ca$ at $E_{lab}(^{16}O)=158.2$ MeV, we have measured elastic, inelastic, and single-nucleon transfer cross sections to resolved final states, and the non-fusion reaction cross section. The measured cross sections to resolved states generally agree with the predicted magnitudes and angular distributions from exact finite-range distorted-wave Born approximation calculations. The total non-fusion reaction cross section, σ_{NF}, is measured to be $0.66^{+0.27}_{-0.07}$ b. These results are compared with other studies made at different bombarding energies, and for other systems.

[NUCLEAR REACTIONS $^{48}Ca(^{16}O,^{16}O)$, $^{48}Ca(^{16}O,^{16}O')$, $^{48}Ca(^{16}O,^{15}N)$, $^{48}Ca(^{16}O,^{17}O)$, $^{48}Ca(^{16}O,X)$, X=Li-Al, $E_{lab}=158.2$ MeV; measured $\sigma(\theta)$, σ_X; optical model and DWBA analysis.]

I. INTRODUCTION

The validity of DWBA as a single-step, direct reaction approximation to heavy-ion-induced inelastic and single-nucleon transfer reactions has been discussed intensively in recent years.[1] A situation where DWBA is expected to adequately describe such reaction data is that of transitions to well-known single-particle states in collisions between closed-shell nuclei. In a previous experiment carried out for the closed-shell system $^{16}O+^{48}Ca$ at $E_{lab}(^{16}O)=56$ MeV,[2] good agreement was found between measured cross sections and DWBA predictions for the inelastic and single-nucleon transfer channels. A question which could not be answered from that experiment is whether DWBA is also able to predict the incident energy dependence of these processes to energies far above the Coulomb barrier. The only other closed-shell system where single-nucleon transfer data exist over a large energy range is $^{16}O+^{208}Pb$.[3,4] Results from the Pb data show serious disagreement with the energy dependence predicted by DWBA, particularly at the higher energies, involving factors of 2 to 3.

In order to test whether similar discrepancies occur for $^{16}O+^{48}Ca$, we have measured inelastic and single-nucleon transfer cross sections for this system at $E_{lab}(^{16}O)=158.2$ MeV. This energy is 4–5 times the Coulomb barrier for $^{16}O+^{48}Ca$ as compared with ~4 times the barrier for the highest energy used in the $^{16}O+^{208}Pb$ study; and it is a factor of ~5 higher at the barrier than for the same system at 56 MeV incident energy.[2] In terms of the relative velocity at the barrier, which may be the parameter more relevant to the reaction behavior, the present experiment has a value ~3 times larger than that of the 56-MeV case, and is about the same as that for the Pb experiment.

We have also measured the non-fusion reaction cross section, σ_{NF}, for $^{16}O+^{48}Ca$ at $E_{lab}(^{16}O)=158.2$ MeV. Our interest in this measurement was to compare the result we obtained at this energy with a previous measurement of σ_{NF} made at $E_{lab}(^{16}O)=56$ MeV,[5] and with fusion cross section data which exist for $^{16}O+^{40}Ca$ over this energy range.[6]

II. EXPERIMENTAL METHODS

The experiment was carried out at Argonne National Laboratory using a ^{16}O beam from the Argonne superconducting linac. The ^{48}Ca target (97.5% enriched) was ~200 $\mu g/cm^2$ thick and was evaporated on a ~20 $\mu g/cm^2$ carbon backing. A self-supporting ~20 $\mu g/cm^2$ carbon target was used to subtract the effects of the carbon backing.

The scattered nuclei were detected in two silicon ΔE-E telescopes. The ΔE and E detector thicknesses were 30 and 500 μm for the more forward angle telescope ($\Delta\Omega=0.059$ msr), and 30 and 300 μm for the more backward angle telescope ($\Delta\Omega=0.216$ msr). The grazing angle at 158 MeV incident energy is $\theta_{lab}\approx 11°$. The measurements were extended in angle to the region where the elastic scattering cross section has dropped to less than

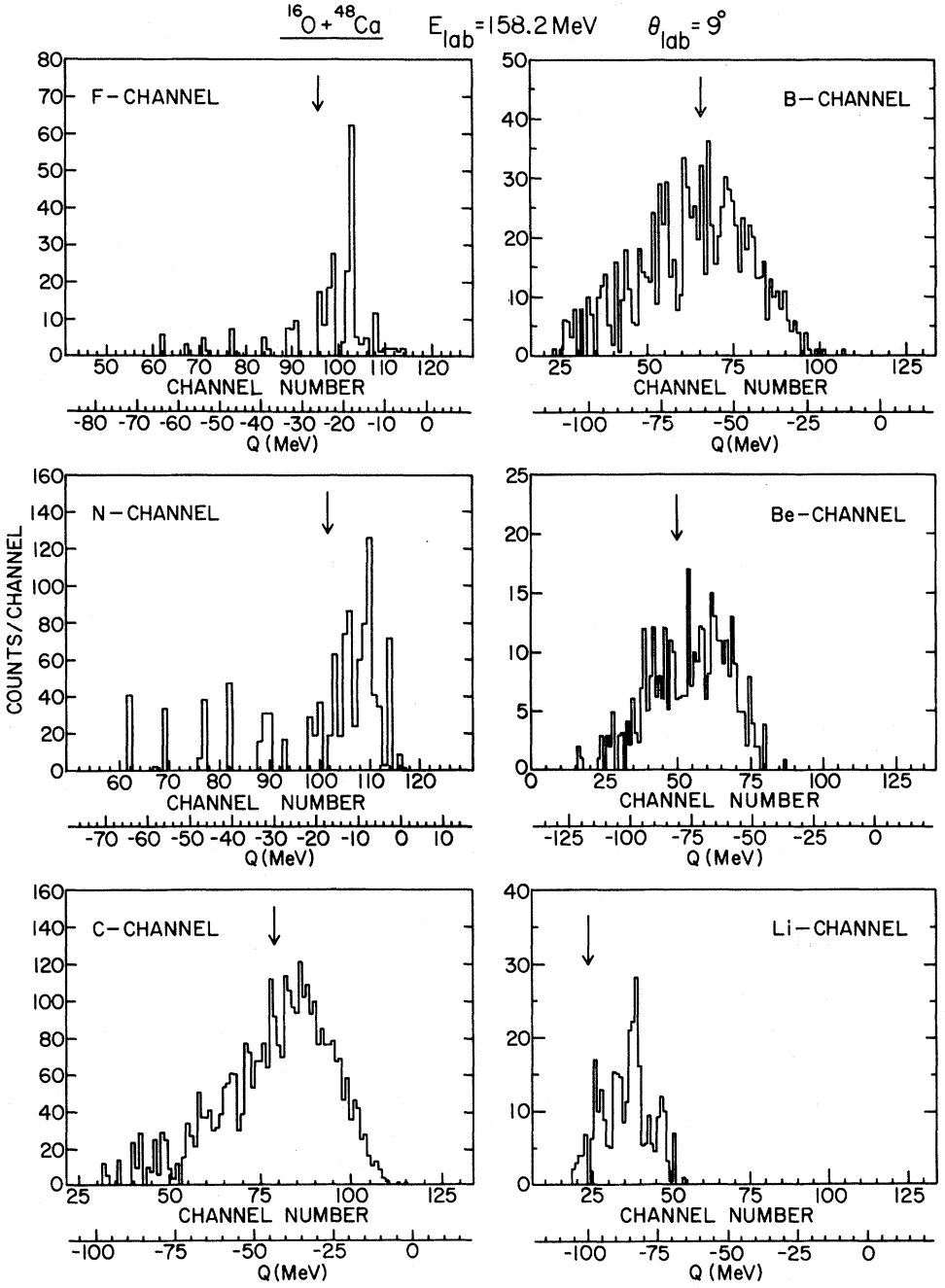

FIG. 1. Energy spectra for different Z channels taken at $\theta_{lab}=9°$. The arrow points to the optimum Q value calculated from Siemens *et al.* (Ref. 16). Note that the high Q value "peaks" in the N-channel spectrum arise from the carbon backing subtraction.

10^{-2} of Rutherford scattering. Thus spectra were measured in the angular range $3° \leq \theta_{lab} \leq 18°$. Figures 1–3 show some representative one-dimensional energy projections. The energy resolution (FWHM) obtained for resolved levels was at best 390 keV and typically $\approx$500 keV (0.3–0.4%).

A silicon monitor detector at 10.5° provided the relative cross section normalization. Absolute cross sections were obtained by normalizing the elastic scattering cross section to Rutherford scattering at $\theta_{lab}=3°$. A 10% uncertainty is estimated in the absolute normalization, resulting from target spot in-

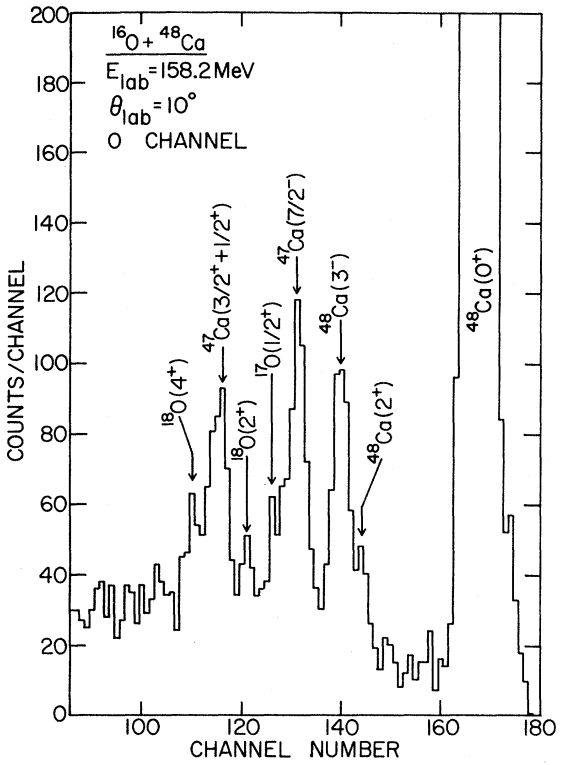

FIG. 2. Energy spectrum for the oxygen channel taken at $\theta_{lab}=10°$ showing elastic, inelastic, and neutron pickup states.

stabilities and angular uncertainties.

III. ELASTIC SCATTERING

Figure 4 shows the experimental elastic scattering angular distribution scaled by Rutherford scattering and an optical model fit to the data. In contrast to the smooth exponential behavior at backward angles observed at 56 MeV,[2] the present data indicate diffractionlike oscillations similar to those seen in $^{16}O+^{40}Ca$ elastic data[6] at similar energies.

The fit to the elastic data was performed with the computer code PTOLEMY,[7] and the optical potential parameters corresponding to the fit shown in Fig. 4 are given in Table I. The potential took the form

$$V(r)=V^c(r)-Vf(r)-iWg(r)\ ,$$

where

$$V^c(r)=\begin{cases}Z_1Z_2e^2/r\ , & r>R_c\\ Z_1Z_2e^2(3-r^2/R_c^2)/2R_c\ , & r<R_c\ ,\end{cases}$$

$$R_c=r_{0c}(A_1^{1/3}+A_2^{1/3})\ ,$$

$$f(r)=\left[1+\exp\left[\frac{r-R_r}{a_r}\right]\right]^{-1}\ ,$$

$$R_r=r_{0r}(A_1^{1/3}+A_2^{1/3})\ ,$$

$$g(r)=\left[1+\exp\left[\frac{r-R_i}{a_i}\right]\right]^{-1}\ ,$$

$$R_i=r_{0i}(A_1^{1/3}+A_2^{1/3})\ ,$$

and where (A_1,Z_1) and (A_2,Z_2) refer to the mass and charge of the projectile and target nuclei, respectively. A wide variety of parameter sets fit the experimental data equally well; the parameter set given in Table I resulted from a four-parameter fit varying the potential geometry and choosing as start parameters those of the potential obtained in the $^{16}O+^{48}Ca$ experiment at 56 MeV incident energy[2] (also listed in Table I). All of the potentials which gave good fits to the data had values of a_r and a_i in the range 0.61—0.67, characteristically larger than those obtained at 56 MeV.

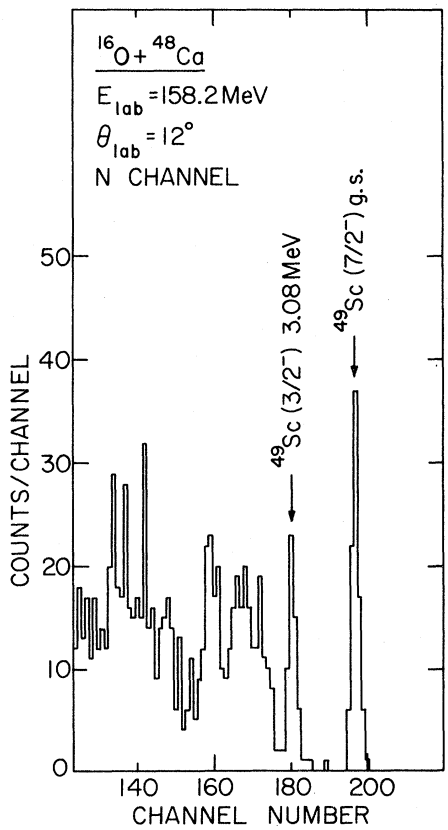

FIG. 3. Energy spectrum for the nitrogen channel taken at $\theta_{lab}=12°$ showing proton stripping states.

TABLE I. Optical-model parameters obtained from a fit to 158.2 MeV elastic scattering data, and from the 56 MeV experiment of Ref. 2.

E_{lab} (MeV)	V (MeV)	r_{0r} (fm)	a_r (fm)	W (MeV)	r_{0i} (fm)	a_i (fm)	r_{0c} (fm)
158.2	100.1	1.063	0.639	24.0	1.207	0.629	1.063
56	100.1	1.200	0.500	24.0	1.207	0.482	1.200

Uncertainties in the measured elastic cross section come from three major sources: (1) the assumption that the cross section at 3° is equal to Rutherford, (2) contamination of the elastic yield at forward angles from ^{40}Ca ($\sim$2%), ^{12}C ($\sim$1%), and ^{16}O ($<$0.5%), and (3) statistics at the backward angles.

IV. EXPERIMENTAL RESULTS FOR TRANSITIONS TO RESOLVED STATES

A. ^{48}Ca(^{16}O,^{16}O')^{48}Ca

The two inelastic states which were observed in this experiment, ^{48}Ca(2$^+$) at 3.83 MeV and ^{48}Ca(3$^-$) at 4.51 MeV, are indicated in Fig. 2, which is an energy spectrum for the oxygen channel at $\theta_{lab}=10°$. Figure 5 shows the measured inelastic angular distributions. The absence of data in the angular region 11°—16° is due to the overlap of the ^{16}O+^{12}C and ^{16}O+^{16}O elastic peaks with the ^{48}Ca inelastic peaks for these angles. The large error bars, which are particularly evident at forward angles, are due to the high background from the elastic scattering tail and errors in separating the incompletely resolved 2$^+$ and 3$^-$ peaks.

The experimental total cross sections for the 2$^+$ and 3$^-$ inelastic channels are found to be 5.7±2.7 mb and 7.8±2.5 mb, respectively. Since the angular regions $\theta_{lab}<3°$ and $\theta_{lab}>18°$ were not measured in the present experiment, it was necessary to estimate these contributions and the resulting uncertainties in them. One way of doing this is to fit an exponential to the measured region and extrapolate to larger and smaller angles. This method finds the

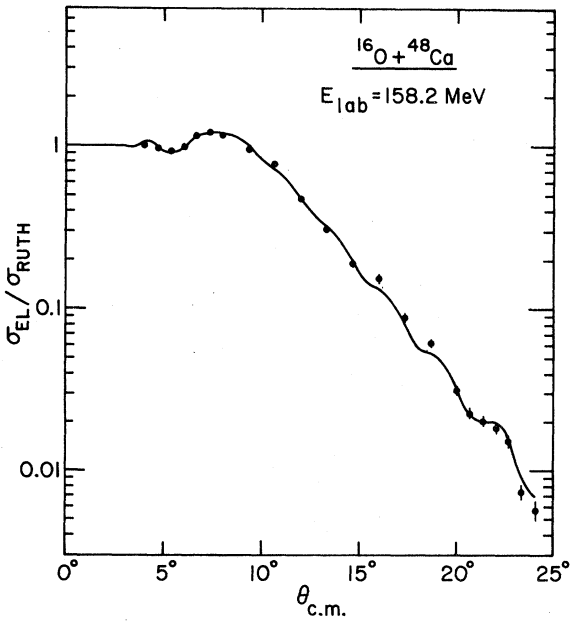

FIG. 4. Elastic scattering angular distribution. The solid line is the optical model fit using the parameters given in Table I.

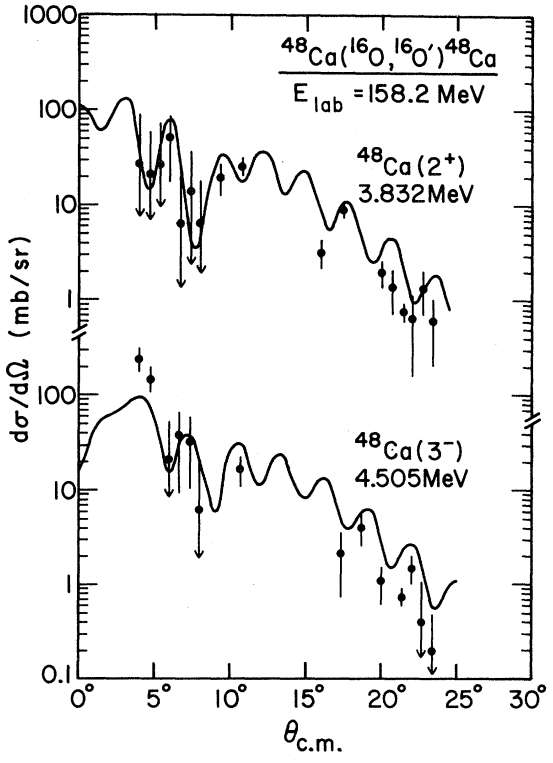

FIG. 5. Inelastic scattering angular distributions for the states ^{48}Ca(2$^+$) and ^{48}Ca(3$^-$). The solid lines are absolute DWBA predictions.

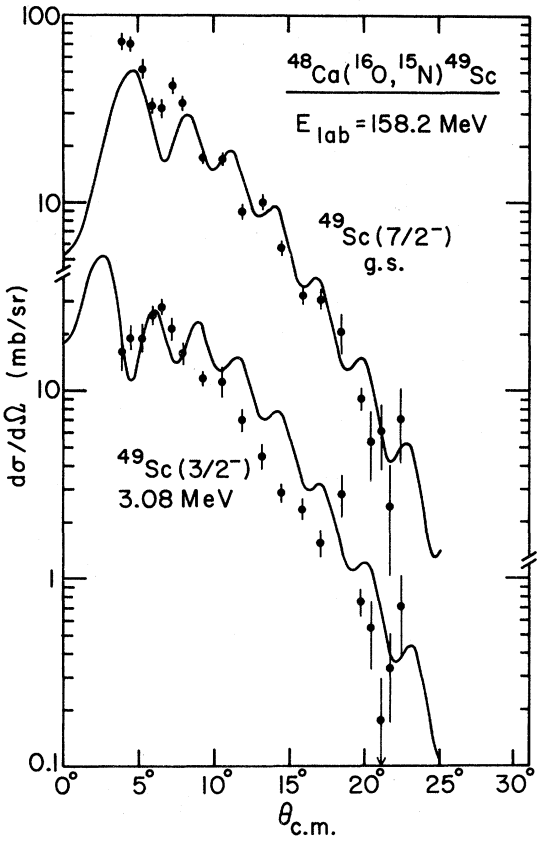

FIG. 6. Proton stripping angular distributions for the states ^{49}Sc($\frac{7}{2}^-$) and ^{49}Sc($\frac{3}{2}^-$). The solid lines are DWBA predictions.

$\theta_{lab} > 18°$ contribution to be $\sim 2\%$ of the total cross section, in agreement with using a DWBA extrapolation, and can therefore be neglected. For $\theta_{lab} < 3°$, this exponential extrapolation is used as an upper limit estimate, a lower limit estimate being obtained from an exponentially decreasing cross section towards zero degrees. The contribution for $\theta_{lab} < 3°$ is thus the average of the upper and lower limits, the uncertainty in this value being the range of the limits. This method was applied to all inelastic and transfer channels, and is found to account for most of the quoted error values for the angle-integrated cross sections.

TABLE II. Deformation parameters used in DWBA calculations for inelastic scattering to the ^{48}Ca(2^+) and ^{48}Ca(3^-) states.

E_{ex} (MeV)	J^π	β_L^c	β_L^N
3.832	2^+	0.103[a]	0.161[b]
4.505	3^-	0.204[a]	0.170[b]

[a]Deduced from (e,e') $B(\mathrm{EL};\uparrow)$ measurements of Ref. 8 using

$$\beta_L^c = 4\pi[B(\mathrm{EL};\uparrow)]^{1/2}/3Z_2e(R_c)^L ,$$

where $R_c = 1.20A_2^{1/3}$.
[b]Fitted value from 56 MeV experiment from Ref. 2.

TABLE III. Spectroscopic factors used in DWBA calculations for ^{48}Ca(^{16}O, ^{17}O)^{47}Ca channels.

^{47}Ca[a]			^{17}O[b]		
E_{ex} (MeV)	J^π	C^2S	E_{ex} (MeV)	J^π	C^2S
0.00	$\frac{7}{2}^-$	6.7	0.00	$\frac{5}{2}^+$	0.81
0.00	$\frac{7}{2}^-$	6.7	0.89	$\frac{1}{2}^+$	0.71
2.59	$\frac{3}{2}^+$	3.4	0.00	$\frac{5}{2}^+$	0.81
2.62	$\frac{1}{2}^+$	1.8	0.00	$\frac{5}{2}^+$	0.81

[a]Reference 9.
[b]References 10 and 11.

B. ^{48}Ca(^{16}O, ^{15}N)^{49}Sc

Figure 3 shows the nitrogen-channel energy projection measured at $\theta_{lab} = 12°$. The single-proton stripping transitions to the $1f_{7/2}$(g.s.) and $2p_{3/2}$(3.08 MeV) single proton states in ^{49}Sc are

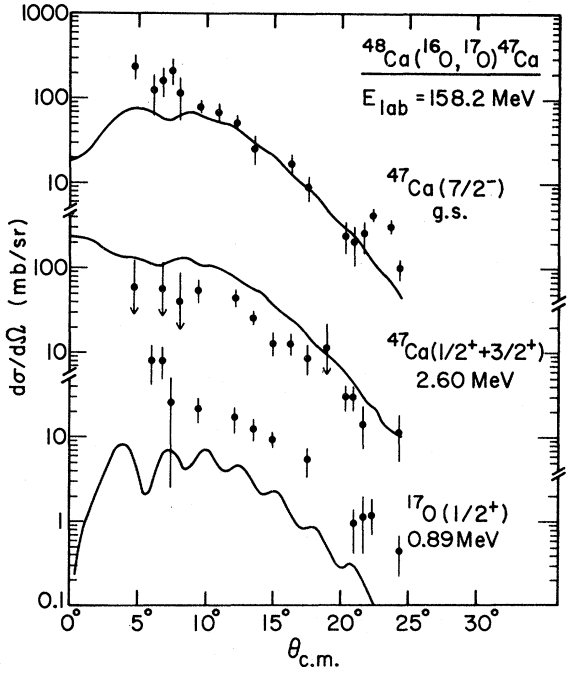

FIG. 7. Neutron pickup angular distributions for the states ^{47}Ca($\frac{7}{2}^-$), ^{47}Ca($\frac{1}{2}^+ + \frac{3}{2}^+$), and ^{17}O($\frac{1}{2}^+$). The solid lines are DWBA predictions.

TABLE IV. Spectroscopic factors used in DWBA calculations for ^{48}Ca(^{16}O,^{15}N)^{49}Sc channels.

^{49}Sc[a]			^{15}N[b]		
E_{ex} (MeV)	J^π	C^2S	E_{ex} (MeV)	J^π	C^2S
0.00	$\frac{7}{2}^-$	1.00	0.00	$\frac{1}{2}^-$	2.00
3.08	$\frac{3}{2}^-$	0.703	0.00	$\frac{1}{2}^-$	2.00

[a]Reference 12.
[b]References 2, 13, and 14.

clearly resolved. The experimental angular distributions for these states, shown in Fig. 6, are observed to have an exponentially decreasing cross section with angle, with oscillations superimposed for the $f_{7/2}$ channel.

The experimental total cross sections for the ^{49}Sc($\frac{7}{2}^-$) and ^{49}Sc($\frac{3}{2}^-$) channels are measured to be 5.5 ± 1.2 mb and 3.0 ± 0.7 mb, respectively.

C. ^{48}Ca(^{16}O,^{17}O)^{47}Ca

Experimental angular distributions of single-neutron pickup (Fig. 7) were extracted for transitions to the $1f_{7/2}{}^{-1}$(g.s.) and unresolved $2s_{1/2}{}^{-1}$ and $1d_{3/2}{}^{-1}$ single-neutron hole states (2.6 MeV) of ^{47}Ca, and the excited projectile state ^{17}O($\frac{1}{2}^+$)$\otimes{}^{47}$Ca($\frac{7}{2}^-$) at 0.89 MeV. The angular distributions are fairly structureless and fall off exponentially with increasing angle.

Since individual masses were not separated in this experiment, the ^{47}Ca($\frac{7}{2}^-$) and ^{47}Ca($\frac{1}{2}^+ + \frac{3}{2}^+$) peaks have contributions of 20–30% from the ^{18}O(0^+) and the ^{18}O(4^+) final states. Since the ^{18}O(2^+) peak could be resolved (see Fig. 2), this yield was used together with the relative two-neutron pickup cross sections measured at 56 MeV for this system[2] to subtract out these background contributions.

The experimental total cross sections for the ^{47}Ca($\frac{7}{2}^-$), ^{47}Ca($\frac{1}{2}^+ + \frac{3}{2}^+$), and ^{17}O($\frac{1}{2}^+$) channels are 23 ± 7 mb, 15 ± 7 mb, and 8.2 ± 3.2 mb, respectively.

V. DWBA ANALYSIS

The main goal of the present work is to investigate the degree of agreement for discrete transitions between DWBA and experiment at 158 MeV incident energy and compare it with that at 56 MeV. It is therefore necessary to carry out the DWBA calculations at 158 MeV in a way that is consistent with the 56 MeV calculations. In order to accomplish this, we have used, wherever possible, the 56 MeV parameters in our DWBA calculations. As a result, only the optical-model parameters shown in Table I differ in the 158 MeV calculations from those at 56 MeV. It should be reemphasized that both sets are the result of optical-model fits to elastic scattering data at the respective energies, and at both energies the entrance and exit channel optical potentials were identical.

The DWBA calculations were performed with the exact finite-range code PTOLEMY.[7] Tables I–IV give some of the parameters used in the calculations. The bound-state parameters used for all of the transfer calculations were the same as at 56 MeV incident energy and are characterized by the following: (1) $r_0=1.25$ fm and $a_0=0.65$ fm, (2) no spin orbit term was included, and (3) the well depth was established using the separation energy prescription. Similar to Ref. 2 we find that varying the bound-state parameters would change the overall normalization of the angular distribution, but not its shape.

A. ^{48}Ca(^{16}O,^{16}O′)^{48}Ca

Figure 5 shows the angular distributions calculated with DWBA for the inelastic channels. Within the relatively large error bars and limited number of data points, the overall magnitude and oscillatory structure is fairly well predicted by DWBA. At backward angles for both states, DWBA tends to slightly overpredict the cross section, as was also seen at 56 MeV.[2]

Table V compares the DWBA and experimental inelastic total cross sections at 158 MeV. For the ^{48}Ca(3^-) channel, agreement within the experimental uncertainty exists, and for the ^{48}Ca(2^+) channel, DWBA predicts a value slightly too high. Note that in order to obtain a reasonable comparison between DWBA and experiment at 158 MeV, the ratio DWBA/Exp in Table V is evaluated by integrating $d\sigma/d\Omega$ over the experimentally-measured angular range $3^\circ \le \theta_{lab} \le 18^\circ$.

B. ^{48}Ca(^{16}O,^{15}N)^{49}Sc

The predicted DWBA angular distributions for the ^{48}Ca(^{16}O,^{15}N)^{49}Sc reactions are shown in Fig. 6. The angular distributions for both the ^{49}Sc($\frac{7}{2}^-$) and ^{49}Sc($\frac{3}{2}^-$) states are predicted to be oscillatory, su-

TABLE V. Comparison of experimental cross sections with DWBA predictions for the $^{16}O+^{48}Ca$ inelastic and transfer channels.

			158.2 MeV		56 MeV[b]		$\frac{\sigma(158.2\text{ MeV})}{\sigma(56\text{ MeV})}$	
Reaction	J^π	E_{ex} (MeV)	σ(Exp) (mb)	$\frac{\text{DWBA}^a}{\text{Exp}}$	σ(Exp) (mb)	$\frac{\text{DWBA}}{\text{Exp}}$	Exp	DWBA
(^{16}O,$^{16}O'$)	2^+	3.832	5.7±2.7	1.6±0.5	6.0 ±0.6	1.2±0.1	1.0±0.5	1.2
(^{16}O,$^{16}O'$)	3^-	4.505	7.8±2.5	1.1±0.2	5.7 ±0.6	1.2±0.1	1.4±0.5	1.1
(^{16}O,^{17}O)	$\frac{7}{2}^-$	0.00	23 ±7	0.6±0.1	10.9 ±1.1	1.0±0.1	2.1±0.7	1.2
(^{16}O,^{17}O)	$\frac{1}{2}^+$	0.89	8.2±3.2	0.2±0.1	0.59±0.06	1.5±0.2	13.9±5.6	1.2
(^{16}O,^{17}O)	$\frac{1}{2}^+ + \frac{3}{2}^+$	2.60	15 ±7	2.0±0.4	1.62±0.16	2.0±0.2	9.3±4.4	7.2
(^{16}O,^{15}N)	$\frac{7}{2}^-$	0.00	5.5±1.2	0.9±0.1	10.3 ±1.0	0.9±0.1	0.5±0.1	0.5
(^{16}O,^{15}N)	$\frac{3}{2}^-$	3.08	3.0±0.7	1.3±0.1	4.9 ±0.5	1.5±0.2	0.6±0.2	0.5

[a]At 158 MeV, DWBA/Exp is evaluated by integrating $d\sigma/d\Omega$ over the measured angular range, i.e., $3° \leq \theta_{lab} \leq 18°$.
[b]From Ref. 2.

perimposed on a more or less exponential falloff with angle. The character of the data is well reproduced by the calculated curves, although there are disagreements in detail. For the $^{49}Sc(\frac{7}{2}^-)$ channel, the oscillatory pattern of the data seems shifted forward in angle relative to that of the DWBA prediction by about 1°, in addition to being underpredicted in magnitude at foward angles. The $^{49}Sc(\frac{3}{2}^-)$ channel data is oscillatory at extreme forward and backward angles, but shows less structure than predicted by DWBA for intermediate angles. In spite of these discrepancies, the quality of the agreement between DWBA and experiment for the (^{16}O,^{15}N) channel angular distributions is quite reasonable and comparable to that seen in the 56 MeV experiment.[2] The cross sections predicted by DWBA for the (^{16}O,^{15}N) channels at 158 MeV are compared with experiment in Table V.

C. $^{48}Ca(^{16}O,^{17}O)^{47}Ca$

Figure 7 shows the angular distributions calculated with DWBA for the $^{48}Ca(^{16}O,^{17}O)^{47}Ca$ channels. The degree to which DWBA is able to describe these channels is similar to that found at 56 MeV.[2] For the $^{47}Ca(\frac{7}{2}^-)$ channel, DWBA correctly predicts the cross section except at the most forward and backward angles. DWBA describes the shape of the $^{47}Ca(\frac{1}{2}^+ + \frac{3}{2}^+)$ channel well, but overpredicts the overall magnitude of the cross section by a factor of 2, as was the case at 56 MeV.[2] A quite different situation occurs for the $^{17}O(\frac{1}{2}^+)$ state, in that the magnitude is underpredicted by a factor of 6, in disagreement with the behavior at 56 MeV (Ref. 2) (see Table V). We have reevaluated our background subtraction which is most critical for the $^{17}O(\frac{1}{2}^+)$ state, but obtain the same result. It may be useful to perform a high-resolution measurement in the near future; the present analysis indicates a failure of DWBA to predict the transfer strength to the ^{17}O excited state. It should be noted, however, that the shape of the angular distribution is described fairly well by DWBA. In Table V, the experimental total cross sections for the (^{16}O,^{17}O) channels are listed together with DWBA predictions.

VI. DISCUSSION OF THE DISCRETE TRANSITIONS

Relatively good overall agreement has been obtained between experiment and DWBA for the $^{16}O+^{48}Ca$ reactions studied in the present work at 158 MeV (Figs. 5–7). The shapes of the experimental angular distributions for all channels are reasonably well reproduced by DWBA, except for disagreements in detail as were discussed in Sec. IV B. From Table V, the measured absolute cross section magnitudes are also rather well reproduced as discussed below in more detail. These results are remarkable considering that all parameters used in the 158 MeV DWBA calculations were the same as those used in the 56 MeV case except for the optical model potential which, however, was completely predetermined by a fit to the elastic scattering at 158 MeV.

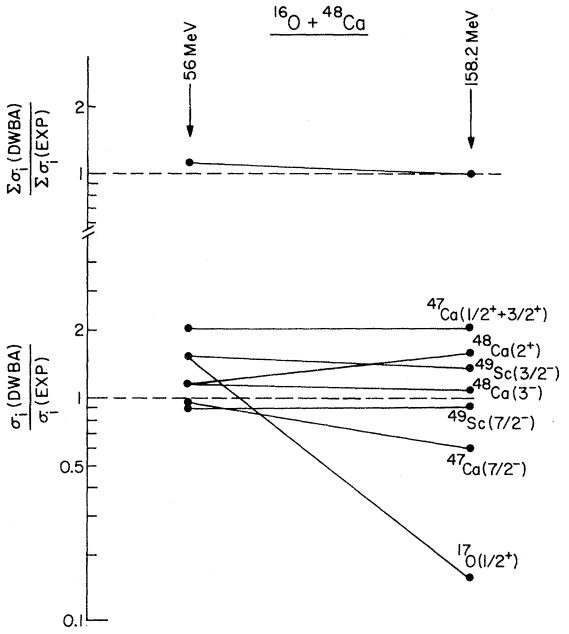

FIG. 8. Graph of $\sigma_i(\text{DWBA})/\sigma_i(\text{Exp})$ at bombarding energies of 56 and 158.2 MeV, with subscripts labeling the states. Also graphed is the ratio of the sum over all states studied.

The largest disagreement between experiment and DWBA found in the 158 MeV measurements occurs for the $[^{16}O, ^{17}O^*(\frac{1}{2}^+)]$ channel. Seglie *et al.*[15] have shown that in the 56 MeV case, this discrepancy can be accounted for using an "effective Q value" which results from molecular-orbital effects during the transfer. In addition, multistep processes which are dependent on kinematics and nuclear structure may be important in these processes.

Along with the total cross sections for 158 MeV, Table V summarizes the results from Ref. 2 for the 56 MeV experiment. For convenience, Fig. 8 plots columns 3 and 6 of Table V. From either Fig. 8 or Table V it is clear that for the $^{16}O+^{48}Ca$ system, the energy dependence predicted by DWBA is consistent with what is found experimentally, at least for the two energies studied. This statement is made more quantitative by considering the ratio $\sigma(158.2\text{ MeV})/\sigma(56\text{ MeV})$ for each channel. As shown in Table V, the experimental value of this ratio agrees with the DWBA calculation for each channel except $[^{16}O, ^{17}O^*(\frac{1}{2}^+)]$. The results for $^{16}O+^{48}Ca$ thus differ greatly from those of the $^{16}O+^{208}Pb$ experiments,[3,4] since in the ^{208}Pb case, each channel studied shows the same systematic energy-dependent discrepancy between DWBA and experiment.

VII. TOTAL NON-FUSION CROSS SECTION

In addition to extracting the yields for transitions to those individual final states that were resolved in our measurement, we have obtained an estimate of the total non-fusion cross section.

Figure 1 shows energy spectra taken at $\theta_{lab}=9°$ for some of the Z channels which were studied, having subtracted the contamination due to the carbon backing of the target. The Q-value scale was calculated assuming two-body kinematics for each channel. The arrow which appears in each energy spectrum in Fig. 1 indicates the optimum Q value for the two-body reaction calculated according to Siemens *et al.*[16] Within the coarse assumption of a particular two-body reaction, the Siemens prescription describes the Z dependence of the optimum Q value rather well for these spectra, indicating the quasielastic nature of these reactions at forward angles.

Figure 9 shows the angular distributions for each Z channel, obtained by integrating over all Q values

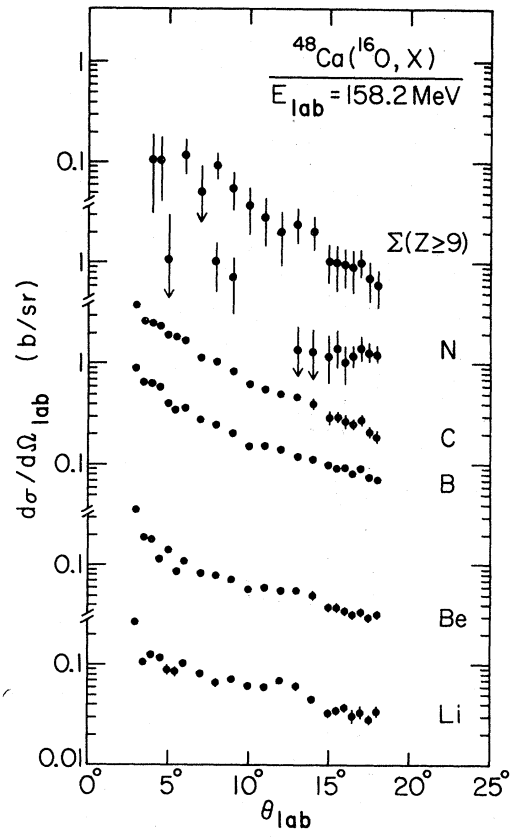

FIG. 9. Measured angular distribution for each Z channel, summed over all Q values.

TABLE VI. Angle-integrated experimental cross sections for each Z channel and summed over Z for $^{16}O+^{48}Ca$, $E_{lab}=158.2$ MeV.

Z Channel	σ_Z (mb)
$\geq$F	130^{+101}_{-21}
O	95^{+71}_{-51}
N	104^{+61}_{-41}
C	213^{+42}_{-22}
B	64^{+27}_{-7}
Be	26^{+24}_{-4}
Li	24^{+24}_{-4}
σ_{NF}[a]	656^{+269}_{-69}
σ_{NF}(56 MeV)	133 ± 20[b]

[a] $\sigma_{NF}\equiv\sum_Z\sigma_Z$.
[b] From Ref. 5.

for each channel. Because of the small cross sections for the fluorine-to-aluminum channels, these channels were summed. In addition to statistical errors, the large error bars seen for nitrogen and $Z\geq9$ result from the subtraction of a large carbon backing contamination ($\sim$50%). The carbon backing contributed less than 10% for the other channels. A reliable value of $d\sigma/d\Omega_{lab}$ for the oxygen channel could only be obtained at back angles; the value obtained was identical within error bars with the nitrogen channel. All angular distributions are seen in Fig. 9 to be rather featureless and more or less exponentially decreasing functions of θ_{lab}, all decreasing at about the same rate.

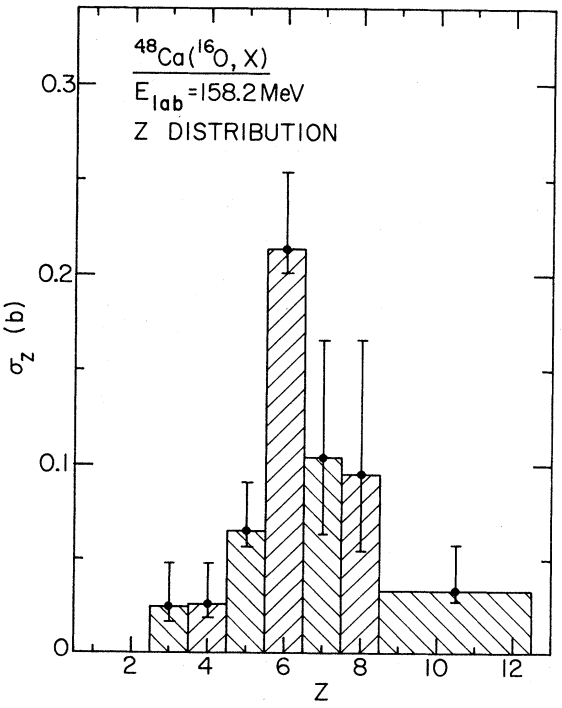

FIG. 10. Non-fusion Z distribution obtained by integrating the angular distributions over θ_{lab}.

The angle-integrated cross section for each Z, σ_Z, is given in Table VI, and plotted in Fig. 10. Two assumptions were necessary in calculating σ_Z from the measured angular distributions: (1) the unmeasured angular regions can be approximated by an exponential, and (2) the oxygen and nitrogen angular distributions have the same shape. Assumption (1) is clearly not valid for far backward angles, where most likely a deep-inelastic component with a $1/\sin\theta$ angular dependence is present. Such $1/\sin\theta$ angular dependences have been seen, particularly at higher energies, for a number of similar systems.[17–19] In order to take into account the possible error in this assumption, we have calculated an upper limit to this effect by assuming a $1/\sin\theta$ dependence for each Z, with 1 mb/sr cross section at 90°, a number in good agreement with upper limits in similar systems.[17–19] This contribution was added to the upper error limit of σ_Z. This is the source of the asymmetric error bars seen in Table VI and Fig. 10. It is argued that assumption (2) is valid on the basis of the systematics seen in Fig. 9.

The carbon channel is seen in Fig. 10 and Table VI to have the largest cross section, being twice as large as nitrogen or oxygen. This is unlike the situation at 56 MeV where, from Ref. 4, carbon is found to be of the same size in cross section as oxygen and nitrogen. The enhancement of carbon production at 158 MeV could be due to increased projectile breakup of ^{16}O into $^{12}C+\alpha$.

The non-fusion reaction cross section, σ_{NF}, defined as

$$\sigma_{NF}=\sum_Z\sigma_Z\ ,$$

is given in Table VI for 158 MeV from the present experiment, and for 56 MeV from Ref. 4. The value of σ_{NF} measured at 158 MeV is seen to be a factor of 5 larger than that measured at 56 MeV.

An estimate of the fusion cross section, σ_{FUS}, can be obtained from σ_{NF} using the relation

$$\sigma_{FUS}=\sigma_R-\sigma_{NF}\ ,$$

where σ_R is the total reaction cross section. Figure 11 shows this graphically, where the solid line is σ_R obtained from optical model calculations, and the lengths of the bars represent σ_{NF} at the two measured energies. The dark portions of the bars give

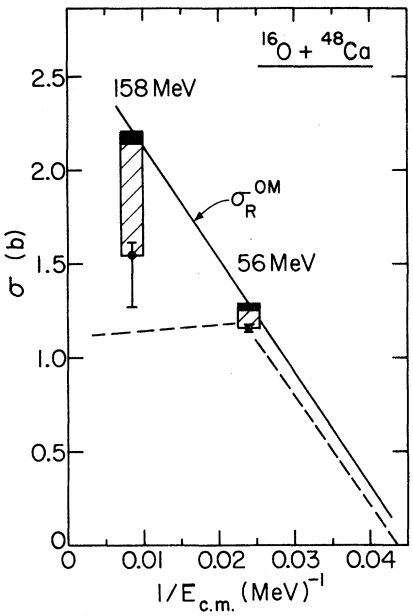

FIG. 11. Graph of σ versus $1/E_{\text{c.m.}}$. The length of the rectangular bar is equal in magnitude to σ_{NF}. The blackened portion of the bar gives the summed contribution to σ_{NF} of the seven resolved states discussed in Sec. IV. The solid line is σ_R calculated from an energy-dependent optical model potential based on the potentials given in Table I at fixed energies. The dashed line shows the trend of the measurements taken by Vigdor *et al.* (Ref. 6) of σ_{FUS} for $^{16}O+^{40}Ca$.

the summed contribution to σ_{NF} of the seven resolved states discussed in Sec. IV. Whereas at 56 MeV these states contributed 30% of σ_{NF}, at 158 MeV they contribute only 9%, suggesting that most of the additional reaction strength present at the higher energy results from the opening of new reaction channels. The dashed line in Fig. 11 reproduces the trend of the measurements of σ_{FUS} for $^{16}O+^{40}Ca$ performed by Vigdor *et al.*[6] in the energy range 40 MeV $\leq E_{\text{lab}} \leq$ 214 MeV. At 56 MeV, the value of σ_{FUS} measured for $^{16}O+^{40}Ca$ is seen to be consistent with what would be expected fc $^{16}O+^{48}Ca$, while at 158.2 MeV, the expected valu of σ_{FUS} for $^{16}O+^{48}Ca$ appears at least 100 ml higher than that measured for $^{16}O+^{40}Ca$. This increase in σ_{FUS} at the higher energy in going from ^{40}Ca to ^{48}Ca is consistent with similar fusion studies which have been carried out on other systems which show that the saturation value in the fusion cross section increases with increasing target neutron number.[20]

We have not considered two processes which can, in principle, effect the measurement of σ_{NF}: (1) fission with subsequent light particle evaporation into nuclei with $Z < 16$, and (2) breakup of projectilelike reaction products into light particles. Fission is judged to be small from the $^{16}O+^{40}Ca$ studies at $E_{\text{lab}} = 140$ MeV.[6] We have assumed that the complete fragmentation yields are small. However, to establish the fusion cross sections, a direct measurement of σ_{FUS} is desirable.

VIII. SUMMARY

We have measured the elastic, inelastic, and single-nucleon transfer cross sections to resolved states, and the total non-fusion cross section for the $^{16}O+^{48}Ca$ system at $E_{\text{lab}}(^{16}O) = 158.2$ MeV.

For the measurements to resolved states, we find in general good agreement between measured cross sections and DWBA predictions at 158.2 MeV, as was found for the lower energy experiment at 56 MeV.[2] This shows that DWBA is able to predict the correct energy dependence for the closed-shell $^{16}O+^{48}Ca$ system, which was found not to be the case for the $^{16}O+^{208}Pb$ system,[3,4] where systematic discrepancies exist between the experimental and DWBA calculated energy dependence. It would clearly be worthwhile to perform similar "high energy" measurements on other systems where good agreement has been obtained between DWBA and experiment at low energies.

The non-fusion cross section, σ_{NF}, has been measured to be a factor of 5 larger at 158 MeV than was found at 56 MeV.[5] This is due to the opening of additional reaction channels at the higher energy such as deep-inelastic reactions and possibly projectile breakup into $^{12}C+\alpha$. From an optical-model estimate of the total reaction cross section, σ_R, and from σ_{NF}, we estimate σ_{FUS} for $^{16}O+^{48}Ca$ to be at least 100 mb larger than for $^{16}O+^{40}Ca$. It would be interesting to measure σ_{FUS} directly for $^{16}O+^{48}Ca$ at 158.2 MeV to compare with the above results.

ACKNOWLEDGMENTS

This work was supported by the U.S. Department of Energy under Contract W-31-109-Eng-38. One of us (H.E.) would like to acknowledge support as an Alexander von Humboldt Foundation Fellow.

[1]See, for example, R. Bass, *Nuclear Reactions with Heavy Ions* (Springer, Berlin, 1980).

[2]D. G. Kovar, W. Henning, B. Zeidman, Y. Eisen, J. R. Erskine, H. T. Fortune, T. R. Ophel, P. Sperr, and S. E. Vigdor, Phys. Rev. C 17, 83 (1978).

[3]Steven C. Pieper, M. H. Macfarlane, D. H. Gloeckner, D. G. Kovar, F. D. Becchetti, B. G. Harvey, D. L. Hendrie, H. Homeyer, J. Mahoney, F. Pühlhofer, W. von Oertzen, and M. S. Zisman, Phys. Rev. C 18, 180 (1978).

[4]C. Olmer, M. Mermaz, M. Buenerd, C. K. Gelbke, D. L. Hendrie, J. Mahoney, D. K. Scott, M. H. Macfarlane, and S. C. Pieper, Phys. Rev. C 18, 2 (1978).

[5]D. G. Kovar, Y. Eisen, W. Henning, T. R. Ophel, B. Zeidman, J. R. Erskine, H. T. Fortune, P. Sperr, and S. E. Vigdor, Argonne National Laboratory Report No. ANL/PHY-76-2, 1976 (unpublished), Vol. II.

[6]S. E. Vigdor, D. G. Kovar, P. Sperr, J. Mahoney, A. Menchaca-Rocha, C. Olmer, and M. S. Zisman, Phys. Rev. C 20, 2147 (1979).

[7]D. H. Gloeckner, M. H. Macfarlane, and S. C. Pieper, Argonne National Laboratory Report No. ANL-76-11, 1976 (unpublished).

[8]R. A. Eisenstein, D. W. Madsen, H. Theisson, L. S. Cardman, and C. K. Bockelman, Phys. Rev. 188, 1815 (1969).

[9]P. Martin, M. Buenerd, Y. Dupont, and M. Chabre, Nucl. Phys. A185, 564 (1973).

[10]F. Ajzenberg-Selove, Nucl. Phys. A166, 1 (1971).

[11]M. D. Cooper, W. F. Hornyak, and P. G. Roos, Nucl. Phys. A218, 465 (1972).

[12]G. Bruge, H. Faraggi, Ha Duc Long, and P. Roussel, Saclay Report No. CEA-N-1232, 124, 1970 (unpublished).

[13]J. C. Hiebert, E. Newman, and R. H. Bassel, Phys. Rev. 154, 898 (1967).

[14]H. Doubre, D. Royer, M. Aediti, L. Bimbot, N. Frascaria, J. P. Garron, and M. Riou, Phys. Lett. 29B, 355 (1969).

[15]E. A. Seglie, J. F. Petersen, and R. J. Ascuitto, Phys. Rev. Lett. 42, 956 (1979).

[16]P. J. Siemens, J. P. Bondorf, D. H. E. Gross, and F. Dickmann, Phys. Lett. 36B, 24 (1971).

[17]L. G. Moretto, R. P. Babinet, J. Galin, and S. G. Thompson, Phys. Lett. 58B, 31 (1975).

[18]R. Albrecht, W. Dünnweber, G. Graw, H. Ho, S. G. Steadman, and J. P. Wurm, Phys. Rev. Lett. 34, 1400 (1975).

[19]T. M. Cormier, A. J. Lazzarini, M. A. Neuhausen, A. Sperduto, K. Van Bibber, F. Videbaek, G. Young, E. B. Blum, L. Herreid, and W. Thoms, Phys Rev. C 13, 682 (1976).

[20]D. G. Kovar, D. F. Geesaman, T. H. Braid, Y. Eisen, W. Henning, T. R. Ophel, M. Paul, K. E. Rehm, S. J. Sanders, P. Sperr, J. P. Schiffer, S. L. Tabor, S. E. Vigdor, B. Zeidman, and F. W. Prosser, Jr., Phys. Rev. C 20, 1305 (1979).